Proceedings of the ASME 2020
Dynamic Systems and Control Conference
DSCC2020
October 5-7, 2020, Virtual, Online

DSCC2020-3335

SAFE DECISION AND CONTROL OF CONNECTED AUTOMATED VEHICLES FOR AN UNPROTECTED LEFT TURN

Sanghoon Oh[1], **Linjun Zhang**[2], **Eric Tseng**[2], **Wayne Williams**[2], **Helen Kourous**[2], **Gabor Orosz**[1,3]
[1]Department of Mechanical Engineering, University of Michigan, Ann Arbor, MI
[2]Ford Motor Company, Dearborn, MI
[3]Department of Civil and Environmental Engineering, University of Michigan, Ann Arbor, MI

ABSTRACT

The unprotected left turn of a connected automated vehicle (CAV) is investigated when it has a potential conflict with a connected human-driven vehicle (CHV) approaching in the opposite lane. A control architecture is proposed that includes interactions between the decision making, motion planning, and control levels. By utilizing the road context and information received via vehicle-to-everything (V2X) communication, a reduced state space representation is determined which allows the CAV to evaluate safety in a fast and efficient manner. Using a temporal metric, a safety evaluation algorithm is developed which determines the safety of the decision making at controller level. To evaluate the algorithms, data collected with real vehicles is utilized.

1 INTRODUCTION

During the last decade there have been considerable development in the area of decision making and control of automated vehicles. A typical control system architecture has hierarchical structure consisting of decision making, motion planning, and vehicle control [1, 2]. Automated vehicles need to interact with other road participants whose motion may conflict with that of the automated vehicle. Such conflicts may be avoided at the decision making level [3–5], at the motion planning level [6–8], and at the control level [9–11]. However, very little research exists on the crosstalk between the different levels of the controls architecture. In this paper we focus on this challenging problem.

In particular, we investigate the scenario when the automated vehicle is executing an unprotected left turn, resulting in potential conflict with an upcoming human-driven vehicle. We assume that both vehicles are equipped with wireless vehicle-to-everything (V2X) communication and refer to them as connected automated vehicle (CAV) and connected human-driven vehicle (CHV). This allows the CAV to respond to the motion of the CHV even when the CHV is beyond the line of sight of the sensors of the CAV. We remark that the feasibility of V2X-based control of CAVs has been recently demonstrated experimentally using real vehicles on public roads [12].

In the left turn scenario the CAV can utilize V2X communication to sense and predict the motion of the oncoming CHV and make decisions to avoid conflict based on the information received. In particular, we define a conflict zone of finite size around the intersection of the predicted path of the CHV and the planned path of the CAV that shall not be shared with the two vehicles at the same time. In order to achieve this we establish a metric called time of share (TOS) that shall be kept negative in order to avoid conflict. A similar concept appeared [13] where a temporal window to pass an intersection was considered. Here we will use TOS in order to establish cross talk between the different levels of the control architecture and improve safety in decision making.

The rest of the paper is organized as follows. In Sec. 2 we specify the left turn scenario and provide a sketch of the system architecture. In Sec. 3 we describe the concept of state space modeling and reduction followed by the details of decision making, trajectory planning and control design. We end this section with the TOS-based safety evaluation that links the controller level to the decision making level. Sec. 4 is devoted to the theoretical and experimental results while we conclude our work and point out future research directions in Sec. 5.

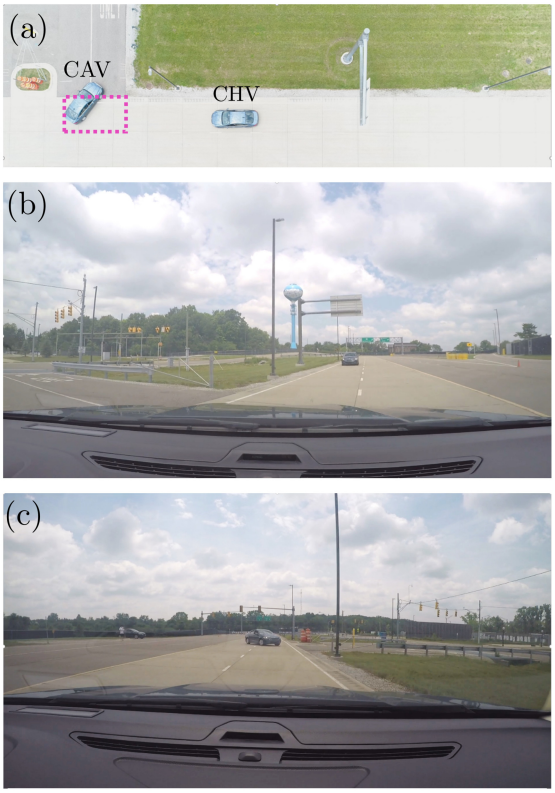

FIGURE 1. UNPROTECTED LEFT TURN SCENARIO. (a) AREAL VIEW INDICATING THE CONFLICT ZONE (MAGENTA RECTANGLE), THE TURNING VEHICLE (CAV), AND THE ONCOMING VEHICLE (CHV), (b) DASHBOARD VIEW OF THE TURNING VEHICLE (CAV), (c) DASHBOARD VIEW OF THE ONCOMING VEHICLE (CHV).

2 PROBLEM SETUP

In this section we describe the unprotected left turn scenario and the proposed control architecture. More technical details will be provided in the next section.

Figure 1 depicts the left turn scenario with real vehicles at the University of Michigan test track called Mcity. The turn is made by the CAV at an unsignalized intersection while the CHV is approaching on the opposite lane. Panel (a) shows an areal photo taken by a drone while panels (b) and (c) show the drivers' views through dash cameras. We remark that when taking these pictures both vehicles were in fact driven by human drivers while being equipped by V2X devices (i.e., they were both CHVs). We remark that the V2X communication allows the CAV to obtain accurate motion information (e.g. position and velocity) about the CHV for a few hundreds of meters and use this information for decision making and control. This cannot be achieved using sensors. More details about the collected data will be given Sec. 4.

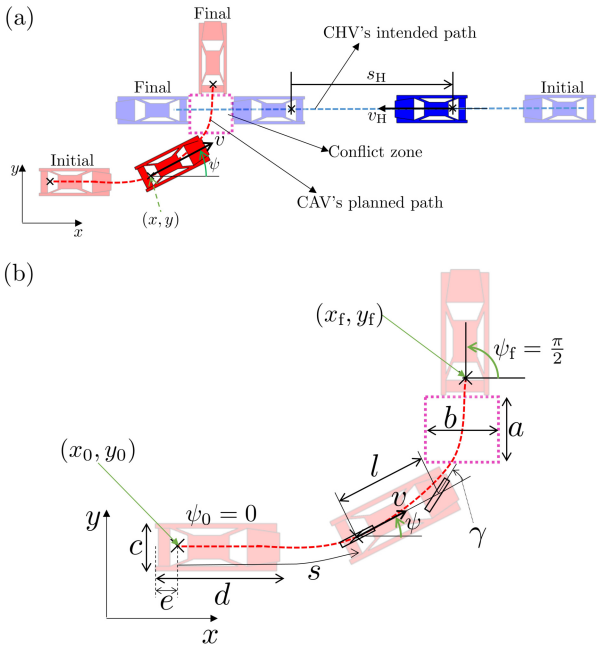

FIGURE 2. (a) LAYOUT OF THE LEFT TURN SCENARIO WITH THE STATE SPACE VARIABLES INDICATED. (b) MECHANICAL MODEL OF THE CAV HIGHLIGHTING THE INITIAL, AN INTERMEDIATE, AND THE FINAL POSITION ALONG THE PLANNED PATH. THE CONFLICT ZONE IS INDICATED WITH THE MAGENTA RECTANGLE.

The conflict zone (magenta rectangle) in Fig. 1(a) is drawn around the point where the vehicles' paths intersect. It is fixed to the road and it can be included in the CAV's digital map. If the two vehicles appear in the this zone at the same time then we say that a conflict occurs that compromises the vehicles' safety. Indeed, the CAV may avoid conflict by waiting the CHV to pass through the conflict zone before moving into the zone. However, waiting for the CHV to pass when a turn can be safely executed reduces the efficiency of the CAV: if the opposite lane carries heavy traffic the CAV may need to stay a long time at the intersection. Thus, the objective of the CAV is chosen to make a non-conflicting turn in minimum time.

The sketch in Fig. 2(a) models the scenario pictured in Fig. 1 with more technical details presented. The CAV is described by three configuration coordinates: the location of the center of its rear axle (x,y) and the yaw angle ψ. In addition, the speed of the center of the rear axle is denoted by v. Notice that the velocity of this point is aligned with the center line of the vehicle as we assume no lateral tire deformations. When considering the CHV only the longitudinal motion is of relevance. Thus, this vehicle can be described by giving the distance s_H of the rear axle from the conflict zone (magenta rectangle) and the longitudinal velocity v_H.

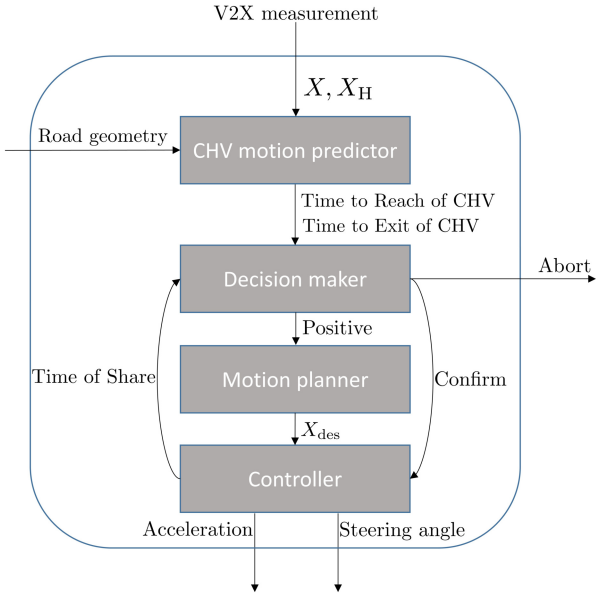

FIGURE 3. SKETCH OF THE SYSTEM ARCHITECTURE. THE CONTROLLER EVALUATES THE BEHAVIORAL DECISION MADE AT THE DECISION MAKING LAYER BY COMPUTING TIME OF SHARE.

Fig. 2(b) provides more details about the CAV's motion including its initial position $(x_0, y_0) = (0,0)$ and orientation $\psi_0 = 0$ and its final position $(x_{\mathrm{f}}, y_{\mathrm{f}}) = (9.8, 7.9)$m and orientation $\psi_{\mathrm{f}} = \pi/2$. We remark that the initial speed is zero $v_0 = 0$ while the final speed is set to $v_{\mathrm{f}} = 5$m/s. Moreover, the size of the conflict zone $a = 3.8$m, $b = 6.4$m and the size of the vehicle $c = 1.8$m, $d = 4.8$m are given together with the distance of the rear axle from the rear bumper $e = 1$m and the wheel base $l = 2.85$m. The steering angle γ is also indicated in the figure. The vehicle is shown following a planned path and the distance travelled by the center of the rear axle is highlighted by s. Indeed, we have $\dot{s} = v$. Specific values of s are related to the cases when the CAV enters the conflict zone $\underline{s}$ and when it exist it $\overline{s}$ (the latter corresponding to the final state). For the optimal trajectory (derived further below) we have $\underline{s} = 6.8$m and $\overline{s} = 14.5$m.

In order to achieve safe and efficient left turn while utilizing V2X connectivity we propose the control architecture for the CAV as shown in Fig. 3. This consists of four consecutive modules: (1) motion predictor for the CHV, (2) decision maker, (3) motion planner, (4) controller. While the detailed description of each layer is presented in Sec. 3, here we highlight the connections between them. Each block feeds into the block below which is a typical scenario for automated vehicles. However, in addition to this, the controller links back to the decision maker and provides its estimation about the time of share (TOS) of the conflict zone. This may allow the decision maker to abort or confirm the decision.

3 MODELING AND CONTROL ARCHITECTURE

In this section we describe the state space modeling and reduction as well as we provide the details of modules in Fig. 3.

3.1 State space modeling and reduction

As described above the system represented in Fig. 2(a) can be described using a six-dimensional state space corresponding to the two variables used to describe the CHV $X_{\mathrm{H}} = [s_{\mathrm{H}}, v_{\mathrm{H}}]^{\mathrm{T}}$ and the four variables used to describe the CAV $X = [x, y, \psi, v]^{\mathrm{T}}$. Searching for maneuvers that avoid conflict in this six-dimensional space would be challenging and it would be particularly difficult to decide what information should be communicated between the modules in Fig. 3. In order to resolve this issue we reduce the state space as described below.

Fig. 4 describes the reduction steps. For the CHV we can utilize the knowledge about its intended path considering the road context as shown in panels (a, b, c). Since we are only interested in when the CHV occupies the conflict zone (even partially) we only need to predict the Time to Reach ($\mathrm{TTR_H}$) and the Time to Exit ($\mathrm{TTR_E}$) for the CHV (rather than predicting the motion of the vehicle as a function of time). These correspond to the time moments when the front bumper of the CHV reaches the zone and when its rear bumper exits it. These may be estimated by using by the position, velocity and acceleration as described further below.

In case of the CAV, as illustrated in Fig. 4(a, d, e), the state space reduction can be done via path planning or trajectory planning. Path planning refers to designing a path in the (x, y)-plane while trajectory planning refers to designing a trajectory in the state space $X = [x, y, \psi, v]^{\mathrm{T}}$. In this paper we choose the latter one. However, once the trajectory is generated it also contains the path and, assuming the vehicle can track the path well, we can describe the motion along the path by using the arclength s and the velocity v. In the reduced state space $\hat{X} = [s, v]^{\mathrm{T}}$ one may identify the arclengths $\underline{s}$ and $\overline{s}$ where the front bumper of the CAV enters the conflict zone and its rear bumper exits the zone, respectively. These correspond to Time to Reach (TTR) and the Time to Exit (TTE) for the CAV.

Finally, one may combine the reduced state space of the CHV and the CAV as shown in Fig. 4(f). In the three-dimensional space $[s, v, t]^{\mathrm{T}}$ the goal is to move "diagonally" while avoiding the conflict cuboid bounded by $s = \underline{s}$, $s = \overline{s}$, $t = \mathrm{TTR_H}$, and $t = \mathrm{TTE_H}$. We remark that the latter two boundaries move based on the updates of the motion prediction of the CHV, and this may require the CAV to re-evaluate its decision as time evolves. The example trajectory in Fig. 4(f) illustrates a case where the CAV enters the conflict set and along the blue portion of the trajectory conflict occurs. This is an example for an unsafe situation that the method presented below tries to prevent.

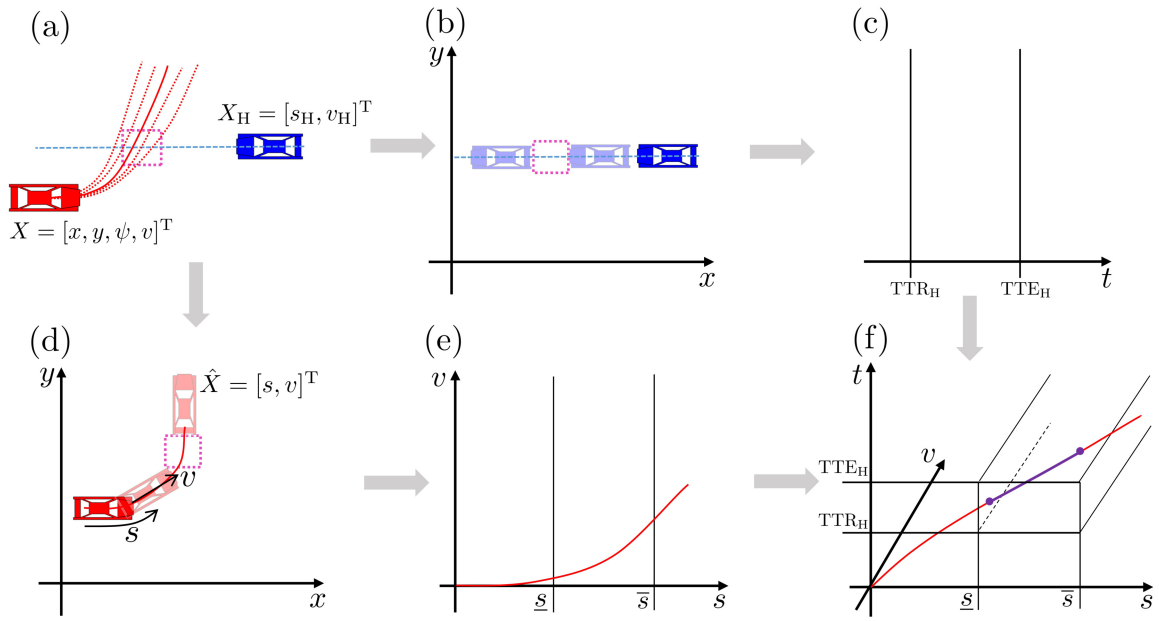

FIGURE 4. DIMENSION REDUCTION OF THE STATE SPACE. (a, b, c): REDUCTION FOR THE CHV USING INTENDED PATH ALONG THE ROAD. (a, d, e): REDUCTION FOR THE CAV USING PLANNED TRAJECTORY. (f) MERGED REDUCED STATE SPACE WITH THE CONFLICT INDICATED BY THE CUBOID. THE BLUE SECTION OF THE TRAJECTORY IS INSIDE THE CUBOID.

3.2 CHV motion prediction and decision making

We assume that the CAV has access to the digital map of the area and monitors the state X_H of the CHV via V2X communication. Then, the goal of the motion prediction module is to predict TTR_H and TTE_H; see Fig. 3. Here we choose a deterministic approach to predict the future motion of the CHV. Since the CHV is traveling on a straight one-lane road and it has the right way, it is assumed that it will continue its way through the intersection (without responding to the CAV who is waiting for making the turn). Moreover, it is assumed that it maintains its current acceleration until it passes through the conflict zone.

Recall that s_H denotes the distance of the rear axle of the CHV from the conflict zone whose length is b; see Fig. 2(a). Also, similar to the CAV, the distance of the rear axle from the rear and front bumpers are e and $d-e$; see Fig. 2(b). These assumptions lead to

$$\mathrm{TTR_H} = \begin{cases} \left(-v_H + \sqrt{v_H^2 + 2a_H(s_H - d + e)}\right)/a_H, & \text{if} \quad a_H \neq 0, \\ (s_H - d + e)/v_H, & \text{if} \quad a_H = 0, \end{cases}$$
$$\mathrm{TTE_H} = \begin{cases} \left(-v_H + \sqrt{v_H^2 + 2a_H(s_H + b + e)}\right)/a_H, & \text{if} \quad a_H \neq 0, \\ (s_H + b + e)/v_H, & \text{if} \quad a_H = 0, \end{cases} \tag{1}$$

where v_H and a_H are the longitudinal velocity of the CHV.

These predictions are fed into the decision making unit in Fig. 3 that is also aware of the state X of the CAV standing at the intersection. If the CAV "thinks" that it can execute its turn before the CHV reaches the conflict zone, based on the state of the CHV X_H (received via V2X) and its own state X, it decides to turn. Otherwise, it stays and waits until the CHV clears the conflict zone. More details about the decision making as a function of s_H and v_H obtained from experiments with human drivers will be given in Sec. 4.

3.3 Motion planning

Once a positive decision is made, the trajectory planning algorithm computes a trajectory in the state space $X = [x, y, \psi, v]^T$ while keeping the inputs $u = [\gamma, a]^T$ bounded. Since our goal is to clear the conflict zone as fast as possible we use the TTE of the CAV as our cost function. We apply the methodology suggested in [14] to rescale time and convert the minimum time problem into a fixed horizon optimal control problem.

As shown in Fig. 2(b) the initial condition of the CAV is given by $X_0 = [x_0, y_0, \psi_0, v_0]^T = [0, 0, 0, 0]^T$, while the desired final state $X_f = [x_f, y_f, \psi_f, v_f]^T = [9.8, 7.9, \pi/2, 5]^T$ corresponds to the case where the CAV's rear bumper leaves the conflict zone. Rather than setting the final state as a boundary condition we include it in the cost function in order to make the corresponding nonlinear optimization problem easier to solve.

Using T for the terminal time we set up the optimal control

problem

$$\min_{u,T} J = T + \big(X(T) - X_\mathrm{f}\big)^\mathrm{T} \mathrm{P} (X(T) - X_\mathrm{f}), \tag{2}$$

subject to

$$\begin{aligned} &\dot{X}(t) = f(X(t), u(t)), \\ &X(0) = X_0, \\ &C(u(t)) \leq 0, \quad 0 \leq t \leq T, \end{aligned} \tag{3}$$

where the dot denotes the derivative with respect to time t. The differential equation $\dot{X} = f(X,u)$ corresponds to the bicycle model

$$\begin{aligned} \dot{x} &= v \cos\psi, \\ \dot{y} &= v \sin\psi, \\ \dot{\psi} &= \frac{v}{l} \tan\gamma, \\ \dot{v} &= a, \end{aligned} \tag{4}$$

where l is the wheelbase, and $C(u) \geq 0$ represents the constraints

$$|\gamma| \leq \gamma_\mathrm{max}, \qquad a_\mathrm{min} \leq a \leq a_\mathrm{max}. \tag{5}$$

Here we use $\gamma_\mathrm{max} = \pi/6$, $a_\mathrm{min} = -8\mathrm{m/s}^2$, $a_\mathrm{max} = 5\mathrm{m/s}^2$. Finally, the cost function contains the positive definite diagonal matrix

$$\mathrm{P} = \begin{bmatrix} (\frac{1}{2.5})^2 & 0 & 0 & 0 \\ 0 & (\frac{1}{2.5})^2 & 0 & 0 \\ 0 & 0 & (\frac{9}{\pi})^2 & 0 \\ 0 & 0 & 0 & (\frac{1}{2})^2 \end{bmatrix}. \tag{6}$$

We rescale time by defining $\sigma = t/T$ and re-write (2,3) as

$$\min_{u,T} J = T + \big(X(1) - X_\mathrm{f}\big)^\mathrm{T} \mathrm{P} (X(1) - X_\mathrm{f}), \tag{7}$$

subject to

$$\begin{aligned} &X'(\sigma) = T f(X(\sigma), u(\sigma)), \\ &X(0) = X_0, \\ &C(u(\sigma)) \leq 0, \quad 0 \leq \sigma \leq 1. \end{aligned} \tag{8}$$

where the prime denotes the derivative with respect to rescaled time σ. We solve this problem by converting it into a nonlinear optimization problem using Euler discretization.

The output of the motion planner is the desired optimal trajectory $X_\mathrm{des} = [x_\mathrm{des}, y_\mathrm{des}, \psi_\mathrm{des}, v_\mathrm{des}]^\mathrm{T}$ and input $u_\mathrm{des} = [\gamma_\mathrm{des}, a_\mathrm{des}]^\mathrm{T}$ that is given to the controller; see Fig. 2.

3.4 Control design and safety evaluation

The goal of the controller module is to track the trajectory provided by the motion planner. The controller module consists of a steering controller that regulates the steering angle and a speed controller that regulates the acceleration. For steering we may use the so-called pure pursuit controller [1], which calculates the steering angle to pursue a selected waypoint with constant radius of curvature. For the low-speed scenarios considered here, this controller is able to track the path with little error justifying the assumptions made above for the state space reduction of the CAV. Thus, for the safety evaluation we can focus our attention on the longitudinal controller.

In order to regulate the longitudinal acceleration we use both feedforward and feedback actions. The feedforward part is computed from the planned trajectory and feedback is used for compensating discrepancy between the model used for planning and the actual vehicle. Since we are concerned about low-speed maneuvers, we neglect the resistance terms and represent the longitudinal dynamics of the vehicle by

$$\dot{v} = \mathrm{sat}(a_\mathrm{com}(t - \tau)), \tag{9}$$

where a_com is the commanded acceleration, the sat function saturates a_min and a_max, and τ represents the powertrain delay. This delay is the gives discrepancy compared to the longitudinal part of the bicycle model (4) where a was saturated by (5). Moreover, we utilize the control law

$$a_\mathrm{com} = a_\mathrm{des} + k_\mathrm{p}(v - v_\mathrm{des}), \tag{10}$$

where a_des and v_des are given by the motion planner while the proportional gain is set to $k_\mathrm{p} = 0.9\frac{1}{\mathrm{s}}$.

The decision made at the decision making level may become unsafe at the controller level due to the changing predictions of the CHV's motion and due to imperfect tracking of the planned trajectory. By numerically integrating the delay differential equation (9,10) the controller computes the Time to Exit of the CAV and compares it with the Time to Reach of the CHV. Thus, we can compute the Time of Share as

$$\mathrm{TOS} = \mathrm{TTE} - \mathrm{TTR}_\mathrm{H}, \tag{11}$$

and based on this value the decision can be revised.

If the TOS value is becomes positive the decision maker may decide to abort the maneuver. However, rather than stepping on the brakes immediately, it shall keep the vehicle running with constant speed until the so-called point of no return is reached. Once the vehicle reaches this point an emergency braking must be performed with acceleration a_min in order to stop the vehicle before $s = \underline{s}$ and prevent it envading the conflict zone.

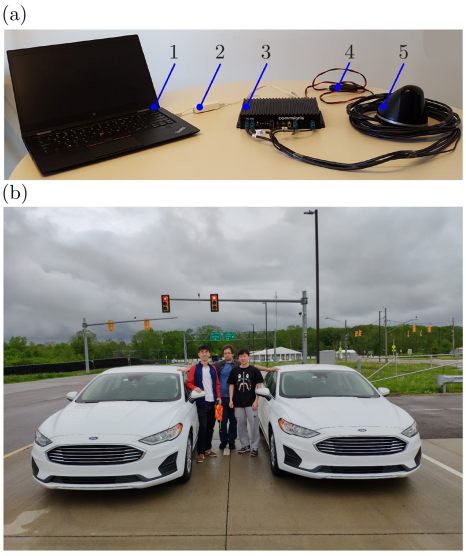

FIGURE 5. (a) MEASUREMENT DEVICE: 1 LAPTOP, 2 ETHERNET CABLE, 3 V2X DEVICE, 4 POWER CABLE, 5 ANTENNA. (b) HUMAN DRIVERS AND CARS USED DURING THE EXPERIMENTS.

The point of no return provides us a boundary at the reduced state space (s, v) of the CAV. In order to calculate this boundary we need to take into account the powertrain delay τ. In particular, to obtain a conservative estimate, we assume that once the emergency braking maneuver is decided the CAV travels with maximum acceleration $a_{\max}$ for τ time before it is able to apply $a_{\min}$. This leads to the formula

$$v(s) = -(a_{\max} - a_{\min})\tau + \sqrt{2a_{\min}(s - \underline{s}) + (a_{\min} - a_{\max})a_{\min}\tau^2}, \tag{12}$$

which can be used in the safety evaluation algorithm to determine whether emergency braking is needed when the TOS becomes positive.

4 RESULTS

In this section, experimental and simulation results are used to demonstrate the concepts presented above. We use experimental data collected with different human drivers to train a decision model. For the motion planner and the controller, numerical simulation is used to evaluate the performance. Combining the experimental data with simulation, the effects of the cross talk between different layers is illuminated.

There are different ways to design decision making algorithms. Here we utilize data collected from human drivers at the test track of the University of Michigan called Mcity. We apply a machine learning based method to find the decision boundary in state space.

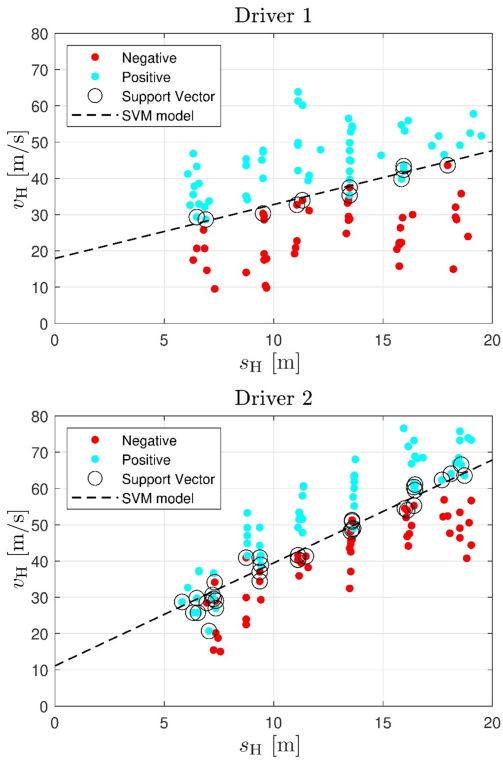

FIGURE 6. SVM CLASSIFICATION RESULTS FOR TWO DIFFERENT DRIVERS.

In order to collect the data we used two human-driven vehicles that were equipped with V2X devices; see Fig. 5. One these CHVs played the role of the CAV by making the left turn while the other CHV was approaching in the opposite lane with constant speed. The driver of the "CAV" was asked to make a turn for different distances s_H and velocities v_H of the approaching CHV. The collected data is summarized in Fig. 6 where positive and negative decisions are differentiated by a color code and clear decision boundaries can be observed.

In order to find the decision boundaries we utilize a supervised learning technique called support vector machine (SVM) used for classification. The SVM classifier gives the hyperplane that maximizes the margin from one class to another. In our case these are lines of the form $v_H = \alpha\, s_H + \beta$ that can be related to the TTE_H in (1) when the CHV had a constant speed. Notice that the line for the two drivers differ significantly: Driver 2 made much more conservative decisions compared to Driver 1 as the latter one was a race car driver.

In order to validate the proposed systems architecture, we compare the algorithm that includes the safety evaluation at the controller level to a so-called "naive" decision algorithm that keeps the initial decision. We generate the CAV's trajectory using the motion planning algorithm presented above and track it using the proposed controller with time delay in the control loop.

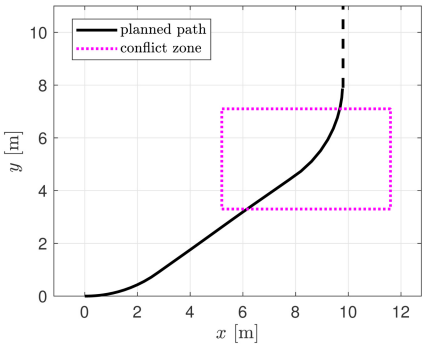

FIGURE 7. PLANNED PATH GIVEN BY THE TRAJECTORY PLANNER (SOLID BLACK CURVE) AND ITS EXTENSION BEYOND THE CONFLICT ZONE (DASHED BLACK LINE).

The optimization problem above generates a trajectory until the CAV exits the conflict zone, i.e., $t \leq T$. The corresponding path is shown by the solid black curve in the (x,y)-plane in Fig. 7. We extend the trajectory by simply adding a straight line motion with $\psi(t) \equiv \pi/2$ and $v(t) \equiv v_{\mathrm{f}}$ for $t > T$ as shown by the dashed section. When re-running the planner from different middle points of the trajectory (starting with velocities that differ from the original plan), we found that the planned path changes very little. We also found that the path can be tracked very closely by using a pure pursuit controller. These justify the proposed state space reduction and the safety evaluations using the longitudinal controller.

Fig. 8 shows the results for a naive decision without the proposed safety evaluation with input delay $\tau = 0.5$s. Based on the decision making boundary of Driver 1 in Fig. 6 we assume that a decision is made when the CHV is $s_{\mathrm{H}} = 43.8$m away from the conflict zone traveling at $v_{\mathrm{H}} = 12.5$m/s and that the CHV maintains this velocity as time evolves. Panels (a) and (b) show the position and the velocity as function of time, while panel (c) shows the trajectory in the three-dimensional state space. The planned trajectories are shown as black (with the part extended beyond the conflict zone being dashed) and they indeed avoid the conflict cuboid in state space. However, due to the delays in the control loop, the actual trajectories, shown as red curves, enter the cuboid as indicated by the blue sections. Using the proposed safety evaluation would result in positive TOS at $t = 0$, and thus, the decision maker would not let the CAV to start the turning maneuver.

Figure 9 shows the simulation result of the proposed decision making algorithm when safety is evaluated at the controller level. The same input delay input $\tau = 0.5$s is considered as in Fig. 8, but it is assumed that the decision is made when the CHV is at $s_{\mathrm{H}} = 43.8$m traveling at $v_{\mathrm{H}} = 11.5$m/s (that is still maintained for the rest of the time). In this case both the planned (not shown) and the actual trajectories are able to avoid the conflict cuboid, and thus, the CAV starts turning at $t = 0$ as indicated by

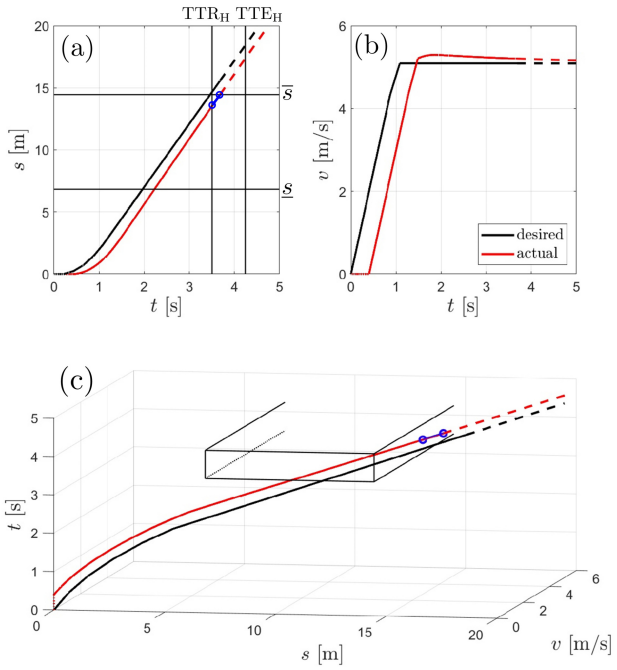

FIGURE 8. SIMULATION RESULTS FOR THE NAIVE DECISION MAKING UNDER INPUT DELAY WITH THE PLANNED TRAJECTORIES (BLACK) AND THE ACTUAL ONES (RED). THE DASHED SECTIONS INDICATE THE MOTION BEYOND THE CONFLICT ZONE WHILE THE BLUE SECTIONS INDICATE CONFLICT BETWEEN THE CAV AND THE CHV. (a) POSITION AS FUNCTION OF TIME. (b) VELOCITY AS FUNCTION OF TIME. (c) TRAJECTORIES IN THE REDUCED STATE SPACE.

the decision on panel (a) corresponding to the negative TOS on panel (b). The corresponding velocity as a function of time is plotted in panel (c) while the trajectory is shown in state space in panel (d).

In order to test the effects of safety evaluations we assume that the V2X packets sent by the CHV are lost for a section of time. The black solid curves in Fig. 9 correspond to having packet loss between $0.9 - 1.2$s while the red dashed curves correspond to having packet loss between $0.9 - 1.5$s. During the packet loss the CHV motion predictor considers the worst case scenario and calculates the $\mathrm{TTR_H}$ assuming that the CHV uses maximum acceleration, i.e., $a_{\mathrm{H}} = a_{\max}$ in (1). Correspondingly the TOS becomes positive in panel (b). Since the CAV has not reached the point of no return estimated by (12), the decision can be kept positive as shown in panel (a). In the short packet loss case, once the communication recovers the TOS becomes negative and the CAV accelerates again to complete the turn. On the other hand, for the long packet loss case the CAV reaches the point no return before the communication recovers and launches an emergency break to come to a halt before $\underline{s} = 6.8$m.

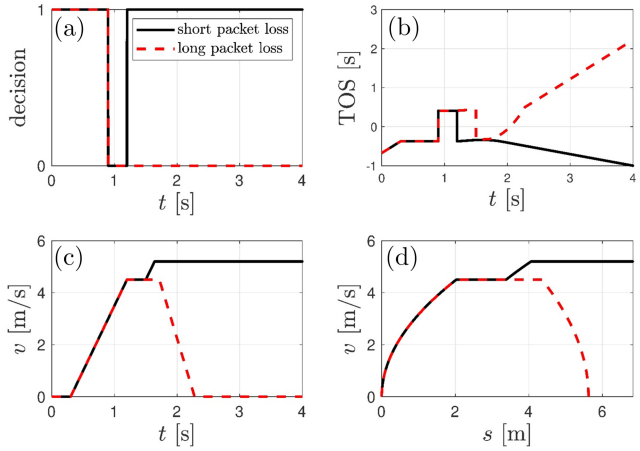

FIGURE 9. SIMULATION RESULTS FOR THE PROPOSED SYSTEMS UNDER INPUT DELAY AND PACKET LOSS. THE SCENARIOS FOR SHORT AND LONG PACKET LOSS ARE DEPICTED AS SOLID BLACK AND RED DASHED CURVES, RESPECTIVELY. (a) DECISION AS FUNCTION OF TIME. (b) ESTIMATED TIME OF SHARE AS FUNCTION OF TIME. (c) VELOCITY AS FUNCTION OF TIME. (d) TRAJECTORIES IN REDUCED STATE SPACE.

5 CONCLUSION

A safe decision making and control strategy was proposed and it was applied to a scenario where connected automated vehicle performed an unprotected left turn while trying to avoid a conflict with an oncoming connected human-driven vehicle. V2X communication was utilized to monitor and predict the motion of the CHV. By utilizing a temporal safety index, the safety of CAV's decision was evaluated at the controller level. It was demonstrated that establishing cross talk between the different levels of the control architecture can help the CAV to avoid conflict with the CHV and improve safety. The proposed algorithms were evaluated with numerical simulations. In the future, the proposed method should be generalized and expanded to various public road scenarios including highway merge, lane change, and other types of unprotected intersection.

REFERENCES

[1] Paden, B., Čáp, M., Yong, S. Z., Yershov, D., and Frazzoli, E., 2016. "A survey of motion planning and control techniques for self-driving urban vehicles". *IEEE Transactions on Intelligent Vehicles,* ***1***(1), pp. 33–55.

[2] Ersal, T., Kolmanovsky, I., Masoud, N., Ozay, N., Scruggs, J., Vasudevan, R., and Orosz, G., 2020. "Connected and automated road vehicles: state of the art and future challenges". *Vehicle System Dynamics,* ***58***(5), pp. 672–704.

[3] Hubmann, C., Becker, M., Althoff, D., Lenz, D., and Stiller, C., 2017. "Decision making for autonomous driving considering interaction and uncertain prediction of surrounding vehicles". In IEEE Intelligent Vehicles Symposium, IEEE, pp. 1671–1678.

[4] Liu, W., Kim, S.-W., Pendleton, S., and Ang, M. H., 2015. "Situation-aware decision making for autonomous driving on urban road using online POMDP". In IEEE Intelligent Vehicles Symposium, IEEE, pp. 1126–1133.

[5] Brechtel, S., Gindele, T., and Dillmann, R., 2014. "Probabilistic decision-making under uncertainty for autonomous driving using continuous POMDPs". In 17th IEEE International Conference on Intelligent Transportation Systems, IEEE, pp. 392–399.

[6] Karaman, S., and Frazzoli, E., 2011. "Sampling-based algorithms for optimal motion planning". *The International Journal of Robotics Research,* ***30***(7), pp. 846–894.

[7] Schmerling, E., Janson, L., and Pavone, M., 2015. "Optimal sampling-based motion planning under differential constraints: the driftless case". In IEEE International Conference on Robotics and Automation, IEEE, pp. 2368–2375.

[8] Reif, J., and Sharir, M., 1994. "Motion planning in the presence of moving obstacles". *Journal of the Association for Computing Machinery,* ***41***(4), pp. 764–790.

[9] Falcone, P., Borrelli, F., Asgari, J., Tseng, H. E., and Hrovat, D., 2007. "Predictive active steering control for autonomous vehicle systems". *IEEE Transactions on Control Systems Technology,* ***15***(3), pp. 566–580.

[10] Gao, Y., Lin, T., Borrelli, F., Tseng, E., and Hrovat, D., 2010. "Predictive control of autonomous ground vehicles with obstacle avoidance on slippery roads". In ASME Dynamic Systems and Control Conference, pp. 265–272.

[11] Nilsson, P., Hussien, O., Balkan, A., Chen, Y., Ames, A. D., Grizzle, J. W., Ozay, N., Peng, H., and Tabuada, P., 2016. "Correct-by-construction adaptive cruise control: Two approaches". *IEEE Transactions on Control Systems Technology,* ***24***(4), pp. 1294–1307.

[12] Ge, J. I., Avedisov, S. S., He, C. R., Qin, W. B., Sadeghpour, M., and Orosz, G., 2018. "Experimental validation of connected automated vehicle design among human-driven vehicles". *Transportation Research Part C,* ***91***, pp. 335–352.

[13] C. Urmson et al., 2008. "Autonomous driving in urban environments: Boss and the urban challenge". *Journal of Field Robotics,* ***25***(8), pp. 425–466.

[14] Park, H., Kolmanovsky, I., and Sun, J., 2014. "Parametric integrated perturbation analysis-sequential quadratic programming approach for minimum-time model predictive control". *IFAC Proceedings Volumes,* ***47***(3), pp. 1922–1927.